atmosphere

MDPI

Article

Impacts of the Wave Train along the Asian Jet on the South China Sea Summer Monsoon Onset

Li Xu and Zi-Liang Li *

College of Oceanic and Atmospheric Sciences, Ocean University of China, Qingdao 266100, China; xuliyir@stu.ouc.edu.cn
* Correspondence: liziliang@ouc.edu.cn

Abstract: The South China Sea (SCS) summer monsoon (SCSSM) onset signifies the commencement of large-scale summer monsoon over East Asia and the western North Pacific (WNP). Previous studies on the influencing factors of the SCSSM onset mainly focus on the tropical systems, such as El Niño-Southern Oscillation (ENSO). This study reveals that the wave train along the Asian jet could act as an extratropical factor to modulate the SCSSM onset, and it is largely independent of ENSO. The SCSSM onset tends to be earlier during the positive phase of the wave train (featured by northerly anomalies over Central Iran plateau and eastern China, southerly anomalies over Arabian Peninsula, eastern Indian subcontinent, and eastern Bonin islands). The wave train affects the SCSSM onset mainly via modulating the WNP subtropical high. The wave train during the positive phase can induce negative geopotential height anomalies in the mid-troposphere and anomalous cyclones in the lower-troposphere over the SCS and the Philippine Sea, leading to the weakening of the WNP subtropical high. Specifically, the anomalous ascending motions associated with the low-level cyclone are favorable for the increased rainfall over the SCS, and the anomalous westerly on the south of the anomalous cyclone is conducive to the transition of the zonal wind (from easterly to westerly). The above circulation anomalies associated with the positive phase of the wave train provide a favorable environment for the advanced SCSSM onset.

Keywords: wave train; Asian jet; South China Sea; summer monsoon onset; the western North Pacific subtropical high

Citation: Xu, L.; Li, Z.-L. Impacts of the Wave Train along the Asian Jet on the South China Sea Summer Monsoon Onset. *Atmosphere* **2021**, *12*, 1227. https://doi.org/10.3390/atmos12091227

Academic Editors: Yangxing Zheng and M. M. Ali

Received: 17 August 2021
Accepted: 17 September 2021
Published: 18 September 2021

1. Introduction

The South China Sea (SCS) is located in the center of the Asian-Australian monsoon, connecting four different monsoon sub-systems: the Indian monsoon, the East Asian monsoon, the Australian monsoon, and the western North Pacific (WNP) monsoon [1]. The South China Sea summer monsoon (SCSSM) onset generally occurs in mid-May around Pentad 28 (16–20 May 2021), which is characterized by a reversal of the low-level easterly to westerly and the abrupt increase in monsoon rainfall [1]. The onset of the SCSSM marks the establishment of the East Asian summer monsoon and the commencement of the major rainy season in East Asia [2–5]. The earlier or later SCSSM onset has essential impacts on summer climate anomalies in East Asia. Previous studies have shown that when the SCSSM onset is earlier (later), drought (flood) is prone to occur along the Yangtze and Huaihe River Basins of China, South Korea, and Japan in summer [6,7]. The earlier or later SCSSM onset can also affect tropical cyclone activities over the WNP. For example, when the SCSSM onset is earlier, it inclines to generate more tropical cyclones over the WNP in May [8]. Many factors can affect the SCSSM onset, such as synoptic-scale systems including tropical cyclones [9,10] and mid-latitude cold fronts [11,12]; tropical intraseasonal oscillations including quasi-biweekly oscillation and 30–60 day oscillation [13,14]; interannual-scale signals including tropical Indian Ocean SST [15], El Niño-Southern Oscillation (ENSO) [16–18], and Arctic Oscillation (AO) [19]. Among them, ENSO is traditionally considered as one of the most important predictors for SCSSM onset [17,18]. The mechanism of El Niño

delaying the SCSSM onset is mainly through regulating Walker circulation [20] and exciting an anomalous anticyclone over the Philippine Sea [17,18,21]. However, previous studies on the impact factors of the SCSSM onset mainly focus on the tropical systems; the extratropical systems affecting the monsoon onset are rarely investigated except for AO and cold fronts.

The wave train, along the Asian jet, as an extratropical system, is the leading model of the empirical orthogonal function (EOF) decomposition for meridional wind anomalies in the upper-troposphere [22,23]. The wave train shows alternate southerly and northerly anomalies along the Asian jet and has an equivalent barotropic structure in the vertical [22–25]. The variability of the wave train can be described by the principal component (PC1) time series of the leading EOF (EOF1) pattern [23,24]. The wave train has important impacts on the Asian summer monsoon circulation system, such as the South Asia high [26] and the WNP subtropical high [27,28]. The wave train can also significantly affect the climate anomalies in East Asia [25,29–32]. For example, the East Asian triple rainfall pattern in summer is closely associated with this wave train [33]. The interdecadal change of the summer precipitation from a meridional triple pattern to a dipole pattern (south-flood-north-drought) over East China around the late-1990s is also related to the wave train [29]. For the SCSSM, the wave train in September can affect the withdrawal of the SCSSM via modulating the South-westerly anomalies over the SCS [34]. The wave train also led to the extremely late SCSSM onset in 2018 [35].

However, the case of the SCSSM onset in 2018 [35] cannot fully reveal the impacts of the wave train along the Asian jet on the SCSSM onset. This study further investigates the statistical relationship between the wave train and the SCSSM onset, as well as the physical mechanism. Section 2 describes the data and methods used in this study. Section 3 investigates the linkage between the wave train and the SCSSM onset and analyzes the possible mechanism of the wave train affecting the SCSSM onset. The conclusions and discussion are presented in Section 4.

2. Data and Methods

The daily and monthly mean atmospheric reanalysis data used in this study are obtained from the National Center for Environmental Prediction/National Center for Atmospheric Research (NCEP/NCAR) reanalysis 1 dataset [36]. The study also uses monthly mean data from the NCEP–Department of Energy (DOE) reanalysis 2 to verify the results obtained from (NCEP/NCAR) reanalysis 1 dataset. The monthly mean Precipitation data is taken from the Monthly Climate Prediction Center (CPC) Merged Analysis of Precipitation (CMAP) dataset [37], which is widely used in the study of the SCSSM [1,19]. The above two datasets have a horizontal resolution of $2.5^\circ \times 2.5^\circ$. The Niño3.4 index is also derived from CPC, which is generally used to represent the ENSO signal [38,39]. The SCSSM onset date is taken from Hu et al. [40]. They determined the SCSSM onset date from six results, which were obtained by applying the same two methods as Kajikawa and Wang [4] and Ding et al. [41] to three kinds of daily reanalysis datasets (NCEP/NCAR, NCEP-DOE, and ERA-Interim). Among these six results, the onset dates had little discrepancies in most years. For the years with large discrepancies, the optimal SCSSM onset date was subjectively determined based on the firm establishment of steady westerly over the SCS. Therefore, the SCSSM onset determined by the above method is more comprehensive and accurate and has been applied to many studies on the SCSSM onset [19,40,42].

The SCSSM onset generally occurs in May; thus, this study focuses on the monthly mean field of May [40,43], and the analyzed period is 1979–2018. In this study, linear correlation coefficient, wavelet coherence, and cross-spectrum analysis [44] are used to analyze the statistical relationship between the wave train and the SCSSM onset. EOF is applied to extract the wave train, and a linear regression analysis is employed to explore the mechanism affecting the SCSSM onset.

3. Results

3.1. The Relationships between the Wave Train along the Asian Jet and the SCSSM Onset

Figure 1 shows wind and geopotential height anomalies in May regressed onto the normalized SCSSM onset date. An anomalous low-level anticyclone appears over the WNP and the SCS, indicating a stronger WNP subtropical high. The anomalous easterly on the south side of this anticyclone can prevent the firm establishment of the low-level monsoonal westerly over SCS, leading to the later SCSSM onset (Figure 1a). In the mid-troposphere, positive geopotential height anomalies appear over the WNP and the SCS, showing a stronger WNP subtropical high (Figure 1b). Namely, the stronger WNP subtropical high can delay the SCSSM onset, while the weaker WNP subtropical high favors the advanced SCSSM onset. The relationships between WNP subtropical high and the SCSSM onset are consistent with previous studies [35,45], indicating the SCSSM onset date employed in this study is reliable.

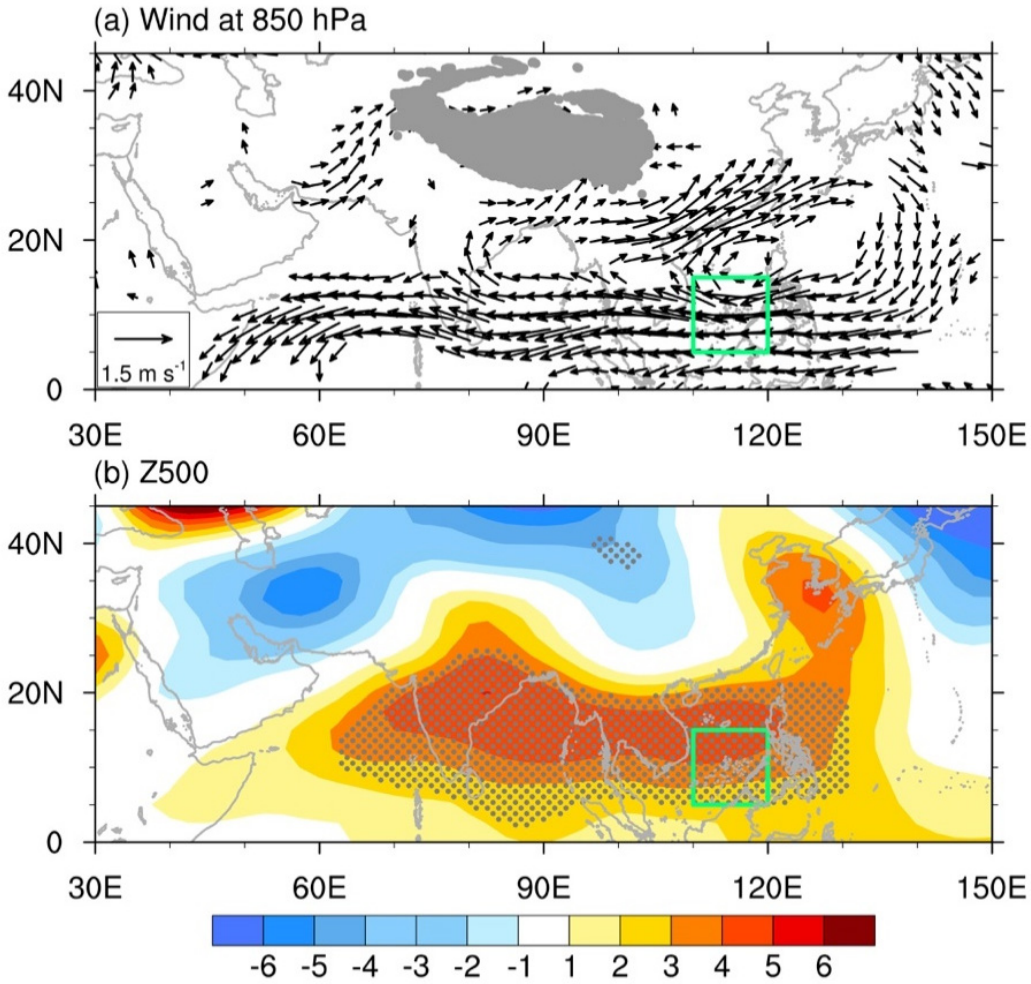

Figure 1. (**a**) Wind at 850 hPa (unit: m s^{-1}) and (**b**) geopotential height anomalies at 500 hPa (unit: gpm) in May regressed onto the normalized time series of the SCSSM onset date for the period of 1979–2018. Only winds that are significant at the 95% confidence level are shown in (**a**). Dotted areas in (**b**) indicate that the regression coefficients are significant at the 95% confidence level. The green rectangles indicate that the region (5° N–15° N, 110° E–120° E) to define the SCSSM onset.

In addition to the stronger WNP subtropical high, the alternating appearance of positive and negative geopotential height anomalies around 30° N is also evident in Figure 1b, which is similar to the mid-latitude wave train. Therefore, there may be some possible linkage between the SCSSM onset and the mid-latitude wave train. Compared

to the geopotential height field, the wave train is more clearly revealed by the meridional wind [22,24]. To confirm the linkage between the mid-latitude wave train and the SCSSM onset, the correlation coefficients between the meridional wind anomalies at 500 hPa in May and the normalized SCSSM onset date are calculated. The layer of 500 hPa is chosen because the subtropical high, as the dominant factor controlling the SCSSM onset [35,45], is more obvious in the mid-troposphere. As shown in Figure 2, southerly and northerly alternately appear along 30° N, showing a clear wave-like structure. Figures 1b and 2 suggest that the mid-latitude wave train may be a possible factor affecting the SCSSM onset.

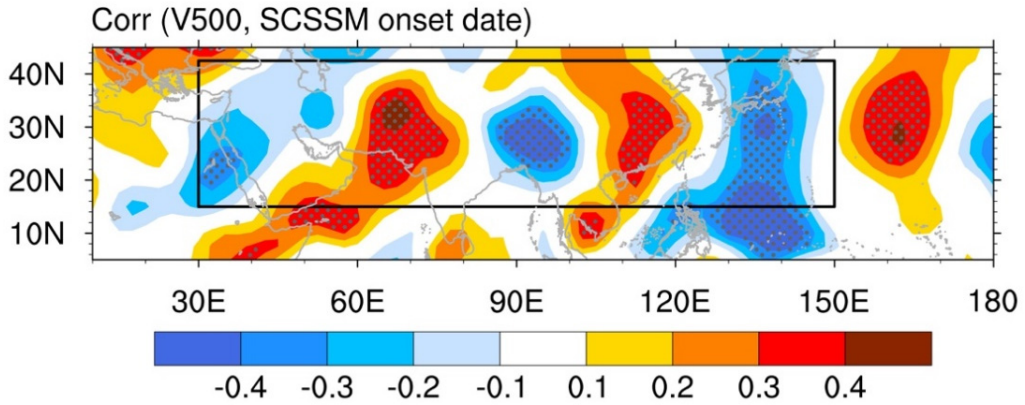

Figure 2. Correlation coefficients between meridional wind anomalies at 500 hPa in May and the normalized time series of the SCSSM onset date for the period of 1979–2018. Dotted areas indicate that the correlation coefficients are significant at the 95% confidence level. The black rectangle denotes the region (15° N–42.5° N, 30° E–150° E) applied to EOF analysis in Figure 3.

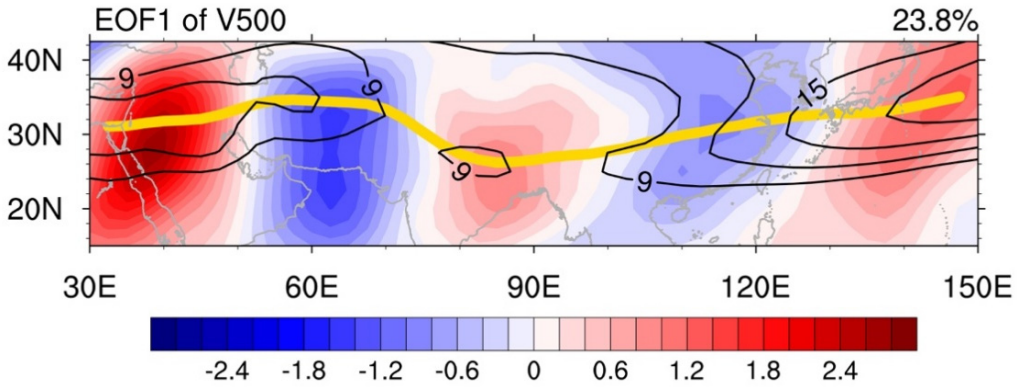

Figure 3. The leading EOF (EOF1) of the meridional wind anomalies (shading, unit: m s^{-1}) at 500 hPa over the domain 15° N–42.5° N, 30° E–150° E and climatological mean zonal wind (contour, contour interval (CI) = 3 m s^{-1})) at 500 hPa in May during 1979–2018. Only the climatological zonal winds speed $\geq$ 9 m s^{-1} are displayed. The thick yellow curve delineates the climatological jet axis.

To determine the statistical relationship between the mid-latitude wave train and the SCSSM onset, EOF analysis is applied to depict this wave train following previous studies [22,23]. Specifically, the EOF analysis is performed for meridional wind anomalies at 500 hPa over the region of 15° N–42.5° N, 30° E–150° E (denoted by the black rectangle in Figure 2). The EOF1 accounts for 23.8% of the total variance and is significantly separated from the other EOF modes, according to North et al. [46]. It is noted that 30° N is exactly the location of the Asian climatological jet axis in May (thick yellow curve in Figure 3). A mid-latitude wave train along the Asian jet is apparent in the EOF1, with northerly anomalies over the central Iranian plateau (around 30° N, 63° E) and eastern China (around 30° N, 115° E), as well as southerly anomalies over the Arabian Peninsula (around 28° N, 40° E), the eastern Indian subcontinent (around 26° N, 85° E), and eastern Bonin Islands

(around 32° N, 143° E), respectively. The above meridional wind anomalies distribution is considered as the positive phase of the wave train along the Asian jet in this study.

The normalized SCSSM onset date, PC1 of meridional wind anomalies at 500 hPa, and the previous winter (DJF) Niño3.4 index is further displayed in Figure 4a. The correlation coefficient between PC1 and the SCSSM onset date is −0.352, which is statistically significant at the 95% confidence level. In addition, the wavelet coherence and cross-spectrum also reveal the out-of-phase relationship between PC1 and the SCSSM onset date (Figure 4b). Namely, corresponding to the positive phase of the wave train, the SCSSM onset tends to be later. While for the negative phase of the wave train, the monsoon onset is likely to be earlier. Because ENSO is an important factor of the SCSSM onset [16–18], we calculated the partial correlation coefficient between PC1 and the SCSSM onset date after removing the ENSO signal. The partial correlation coefficient is −0.324, still significant at a 95% confidence level. In conclusion, the wave train along the Asian jet is an extratropical factor that may modulate the SCSSM onset, and it is largely independent of ENSO.

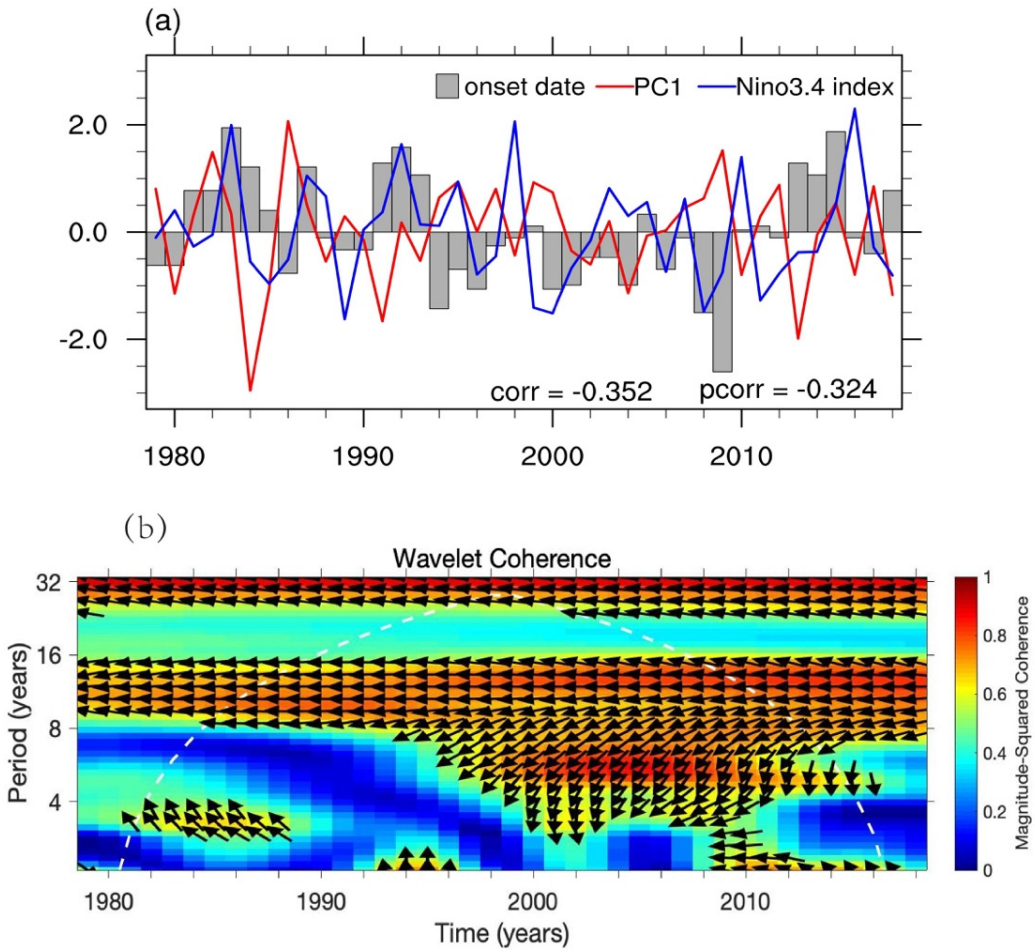

Figure 4. (**a**) The normalized time series of the SCSSM onset date (grey bar), PC1 of meridional wind anomalies at 500 hPa (red line), and the previous winter (December–February, DJF) Niño3.4 index (blue line) during 1979–2018. (**b**) The wavelet coherence and cross-spectrum between the normalized time series of PC1 and the SCSSM onset date.

3.2. Physical Mechanism behind the Relationships

To investigate the mechanism of the SCSSM onset affected by the wave train along the Asian jet, a linear regression analysis is performed to obtain the circulation anomalies associated with the wave train. As shown in Figure 5, a clear wave train can be observed extending eastward from the South-central Mediterranean to East Asia along the Asian jet (nearly 30° N). Taking the positive phase of the wave train as an example, in the upper-

troposphere, there appear positive geopotential height anomalies over Iran and western China. Meanwhile, negative geopotential height anomalies appear over Northeast Africa, Indian Peninsula, and East Asia, respectively. The wave activity flux [47] propagates along the Asian jet eastward from the south-central Mediterranean (Figure 5a). The distribution of geopotential height anomalies and the wave activity flux at 500 hPa are similar to that at 200 hPa, but the significant negative geopotential height anomaly near the Sea of Japan extends South-west to the SCS (Figure 5b). At 850 hPa, except that the negative geopotential height anomaly becomes not obvious in Northeast Africa and disappears in Indian Peninsula, other anomaly centers still exist. Particularly, a negative geopotential height anomaly still extends from the Sea of Japan to the SCS (Figure 5c). The geopotential height anomalies associated with the wave train are similar at different levels, indicating that the wave train has an equivalent barotropic structure in the vertical, which is consistent with previous studies [22,24]. The negative geopotential height anomalies over the WNP and the SCS in May induced by the wave train facilitate the weakening and eastward retreat of the WNP subtropical high, which is an important circulation system for interannual variability of the SCSSM onset [35,45]. Simultaneously, the low-level anomalous cyclone over the Philippine Sea and the SCS also contributes to the weaker WNP subtropical high, and the anomalous westerly on the south of the anomalous cyclone is conducive to the reversal of the low-level wind from easterly to westerly (Figure 5c). Besides, the convergence in the lower-troposphere and the divergence in the upper troposphere over the Philippine Sea are favorable for the anomalous ascending motions, resulting in the weakening of the WNP subtropical high. The weakened WNP subtropical high is favorable for the anomalous westerly into the SCS, contributing to the earlier onset of the SCSSM. In contrast to the positive phase, the negative phase of the wave train is advantageous to the enhancement and westward extension of the WNP subtropical high, which promotes the intrusion of easterly over the SCS, leading to the later onset of the SCSSM.

It is known that the increase in rainfall over the SCS is an important characteristic of the SCSSM onset [1]. The rainfall in May is regressed onto the normalized PC1 to examine the rainfall anomaly induced by the wave train (Figure 6). The regressed rainfall field shows positive anomalies over the SCS, indicating that the positive phase of the wave train is conducive to the occurrence of rainfall over the SCS in May. The positive rainfall anomalies are consistent with the circulation anomalies, which present an anomalous cyclone with the ascending motions over the SCS and the Philippine Sea (Figure 5), promoting the earlier SCSSM onset.

To further confirm, climatological and regressed pentad mean horizontal winds and 850–500 hPa omega are shown in Figure 7. Before calculating the climate average and regression, the data are averaged across the SCS from 110° E to 120° E. The reversal of the wind from easterly to westerly and the establishment of the ascending motions (representing rainfall) between 5° N and 15° N occur in mid-May around pentad 28, namely the climatological SCSSM onset occurs in mid-May around pentad 28 (Figure 7a), which is consistent with previous studies [1,48]. The significant westerly anomalies between 5° N and 15° N occur during pentad 26–29, which favors the establishment of low-level westerly over the SCS (Figure 7b). Meanwhile, gradually enhanced negative vertical velocity anomalies appear during pentad 26–28, which is conducive to the increase in rainfall over the SCS. It is noted that the significant westerly anomalies and the enhanced ascending motions occur over the SCS as early as pentad 26. Therefore, by causing the anomalous westerly and the increase in rainfall over the SCS, the positive phase of the wave train could provide a favorable environment for the advanced SCSSM onset.

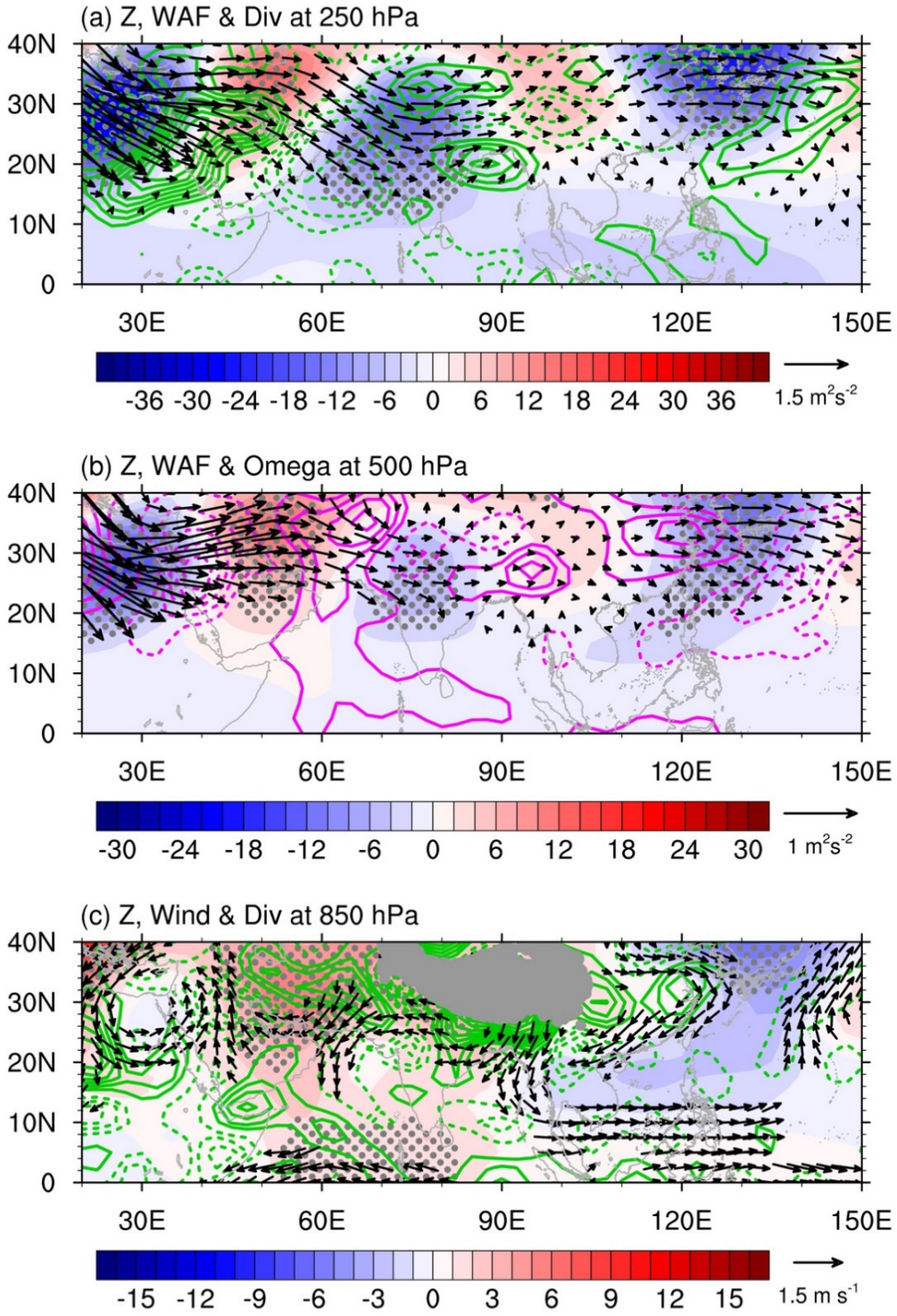

Figure 5. (**a**) Geopotential height anomalies (shading, unit: gpm), wave activity flux (vector, unit: m^2s^{-2}), and divergence (green contour, CI = $0.02\times10^{-5}s^{-1}$) at 200 hPa in May regressed onto the normalized time series of PC1; (**b**) geopotential height anomalies, wave activity flux, and omega (purple contour, CI = 0.004 Pa s^{-1}) at 500 hPa in May regressed onto the normalized time series of PC1; (**c**) geopotential height anomalies, wind (vectors, unit: m s^{-1}), and divergence (green contour, CI = $0.015\times10^{-5}s^{-1}$) at 850 hPa in May regressed onto the normalized time series of PC1. All zero contours are omitted, and the solid (dashed) contours indicate the positive (negative) values. Dotted areas indicate that the regression coefficients of geopotential height anomalies are significant at the 95% confidence level. The grey shading area is the plateaus in (**c**).

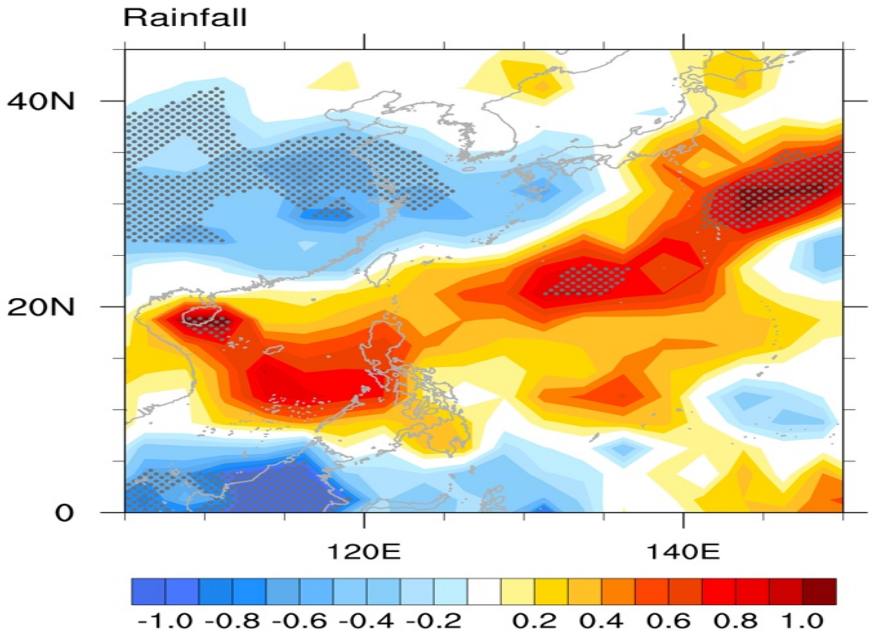

Figure 6. CMAP rainfall (shading, unit: mm day^{-1}) and wind (vectors, unit: m s^{-1}) at 850 hPa in May regressed onto the normalized time series of PC1. Dotted areas indicate that the regression coefficients of rainfall are significant at the 95% confidence level.

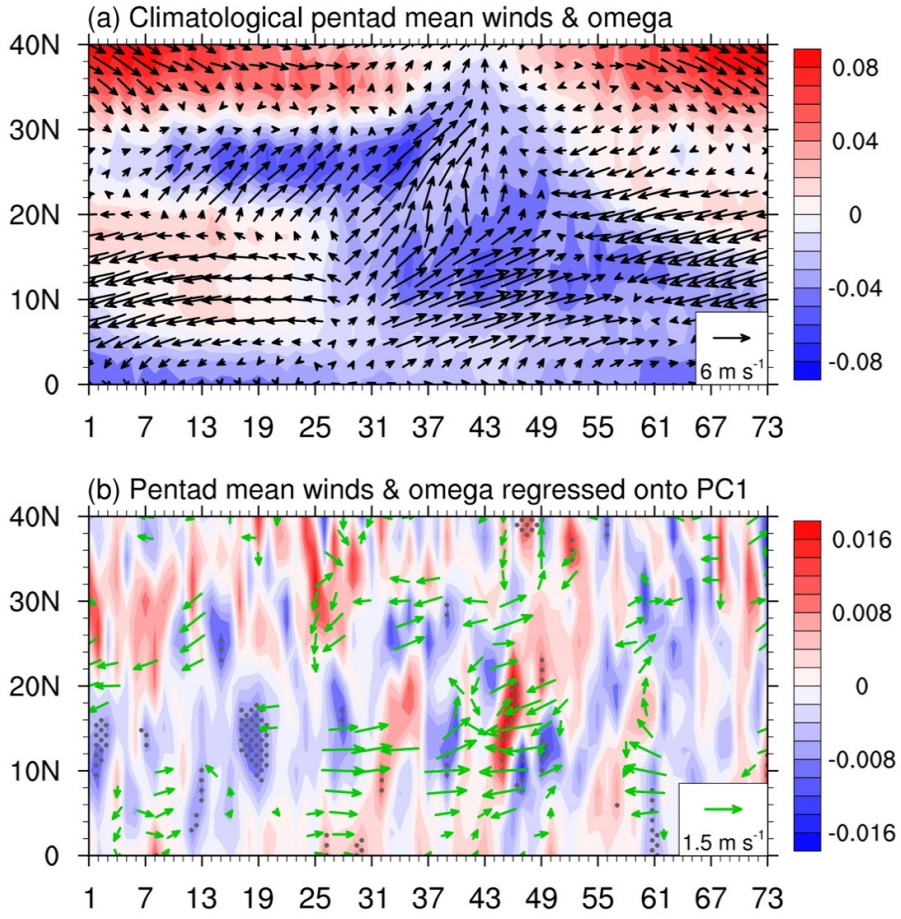

Figure 7. (**a**) Climatological pentad mean horizontal winds (vector, unit: m s^{-1}) and pentad mean 850–500 hPa omega (shading, unit: Pa s^{-1}) for the period of 1979–2018. (**b**) pentad mean horizontal

winds and pentad mean 850–500 hPa omega regressed onto the normalized time series of PC1. The data are averaged across the SCS over the longitude between 110° E and 120° E. Dotted areas and green vectors indicate that the regression coefficient of omega and horizontal winds are significant at the 90% confidence level in (**b**).

4. Conclusions and Discussion

This study reveals that the wave train along the Asian jet could act as an extratropical factor affecting SCSSM onset, which is largely independent of ENSO. In this study, the positive phase of the wave train is characterized by northerly anomalies over the central Iranian plateau and eastern China, and southerly anomalies around the Arabian Peninsula, eastern Indian subcontinent, and eastern Bonin Islands, respectively. The meridional wind distribution of the negative phase is the opposite. The results of the correlation analysis, wavelet coherence, and cross-spectrum analysis show that the SCSSM onset tends to be earlier (later) when the wave train is in the positive (negative) phase.

Figure 8 illustrates the possible mechanism of the SCSSM onset affected by the wave train along the Asian jet in May. Taking the positive phase of the wave train as an example, the wave train could induce the negative geopotential height anomalies over the SCS and the WNP in the mid-troposphere. There also appears to be a significant anomalous cyclone over the SCS and the Philippine Sea in the lower troposphere. Moreover, anomalous ascending motions exist over the SCS and the Philippine Sea. The above circulation anomalies lead to the weakening of the WNP subtropical high. In particular, the anomalous ascending motions are conducive to the occurrence of rainfall over the SCS, and the anomalous westerly on the south side of the anomalous cyclone favors the firm establishment of the westerly. The combined effects of these aspects create a favorable atmospheric environment for the earlier SCSSM onset. The positive phase of the wave train could make the onset date earlier by weakening the WNP subtropical high. Contrary to the positive phase, the negative phase of the wave train could delay the SCSSM onset by strengthening the WNP subtropical high.

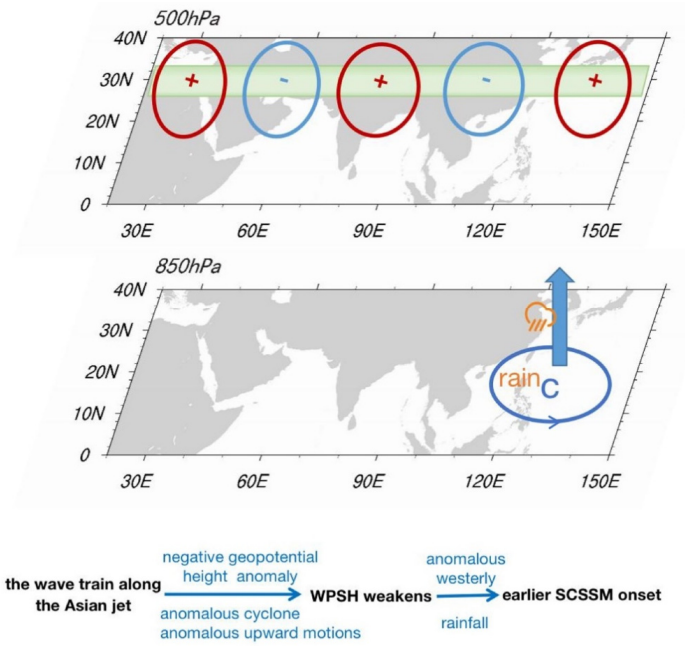

Figure 8. A schematic diagram of the mechanism of the SCSSM onset affected by the wave train along the Asian jet. The "+" and "−" symbols denote southerly anomalies and northerly anomalies at 500 hPa, respectively. The light green shaded belt represents the climatological Asian jet at 500 hPa in May. Letter "C" represents an anomalous cyclone over the SCS and the Philippine Sea. A thick vertical arrow indicates anomalous ascending motions.

This study reveals that the wave train along the Asian jet has impacts on the SCSSM onset, and it is known that the monsoon onset can affect tropical cyclone activities over the WNP. Thus, whether the wave train can affect the generation of tropical cyclones over the WNP needs to be investigated in the future. In this study, the formation and maintenance mechanism of the wave train are not involved, which also need to be investigated in the future.

Author Contributions: L.X. prepared the manuscript, analyzed the data and prepared the figures. Z.-L.L. supervision, revised the manuscript. All authors have read and agreed to the published version of the manuscript.

Funding: This research was funded by the National Key Basic Research and Development Plan of China (Grant No. 2015CB953900). The APC was funded by Z.-L.L.

Institutional Review Board Statement: Not applicable.

Informed Consent Statement: Not applicable.

Data Availability Statement: All data are available to readers upon request.

Acknowledgments: The authors are very grateful to the editor and anonymous reviewers for their help.

Conflicts of Interest: The authors declare no conflict of interest.

References

1. Wang, B.; Huang, F.; Wu, Z.; Yang, J.; Fu, X.; Kikuchi, K. Multi-scale climate variability of the South China Sea monsoon: A review. *Dyn. Atmos. Ocean.* **2009**, *47*, 15–37. [CrossRef]
2. Ding, Y.; Chan, J.C. The East Asian summer monsoon: An overview. *Meteor. Atmos. Phys.* **2005**, *89*, 117–142.
3. Ding, Y.; Wang, Z. A study of rainy seasons in China. *Meteor. Atmos. Phys.* **2008**, *100*, 121–138.
4. Kajikawa, Y.; Wang, B. Interdecadal change of the South China Sea summer monsoon onset. *J. Clim.* **2012**, *25*, 3207–3218. [CrossRef]
5. Ding, Y.; Liu, Y.; Song, Y.; Zhang, J. From MONEX to the global monsoon: A review of monsoon system research. *Adv. Atmos. Sci.* **2015**, *32*, 10–31. [CrossRef]
6. Huang, R.; Chen, J.; Huang, G. Characteristics and variations of the East Asian monsoon system and its impacts on climate disasters in China. *Adv. Atmos. Sci.* **2007**, *24*, 993–1023. [CrossRef]
7. He, J.; Zhu, Z. The relation of South China Sea monsoon onset with the subsequent rainfall over the subtropical East Asia. *Int. J. Climatol.* **2015**, *35*, 4547–4556. [CrossRef]
8. Huangfu, J.; Huang, R.; Chen, W. Relationship between the South China Sea summer monsoon onset and tropical cyclone genesis over the western North Pacific. *Int. J. Climatol.* **2017**, *37*, 5206–5210. [CrossRef]
9. Mao, J.; Wu, G. Influences of Typhoon Chanchu on the 2006 South China Sea summer monsoon onset. *Geophys. Res. Lett.* **2008**, *35*, L12809. [CrossRef]
10. Huangfu, J.; Huang, R.; Chen, W. Statistical analysis and a case study of tropical cyclones that trigger the onset of the South China Sea summer monsoon. *Sci. Rep.* **2017**, *7*, 12732. [CrossRef]
11. Tong, H.W.; Chan, J.C.L.; Zhou, W. The role of MJO and mid-latitude fronts in the South China Sea summer monsoon onset. *Clim. Dyn.* **2009**, *33*, 827–841. [CrossRef]
12. Huangfu, J.; Chen, W.; Wang, X.; Huang, R. The role of synoptic-scale waves in the onset of the South China Sea summer monsoon. *Atmos. Sci. Lett.* **2018**, *19*, e858. [CrossRef]
13. Shao, X.; Huang, P.; Huang, R. Role of the phase transition of intraseasonal oscillation on the South China Sea summer monsoon onset. *Clim. Dyn.* **2014**, *45*, 125–137. [CrossRef]
14. Wang, H.; Liu, F.; Wang, B.; Li, T. Effects of intraseasonal oscillation on South China Sea summer monsoon onset. *Clim. Dyn.* **2018**, *51*, 2543–2558. [CrossRef]
15. Yuan, Y.; Zhou, W.; Chan, J.C.L.; Li, C. Impacts of the basin-wide Indian Ocean SSTA on the South China Sea summer monsoon onset. *Int. J. Climatol.* **2008**, *28*, 1579–1587. [CrossRef]
16. Zhou, W.; Chan, J.C.L. ENSO and the South China Sea summer monsoon onset. *Int. J. Climatol.* **2007**, *27*, 157–167. [CrossRef]
17. Zhu, Z.; Li, T. Empirical prediction of the onset dates of South China Sea summer monsoon. *Clim. Dyn.* **2017**, *48*, 1633–1645. [CrossRef]
18. Martin, G.M.; Chevuturi, A.; Comer, R.E.; Dunstone, N.J.; Scaife, A.A.; Zhang, D. Predictability of South China Sea summer monsoon onset. *Adv. Atmos. Sci.* **2019**, *36*, 253–260. [CrossRef]
19. Hu, P.; Chen, W.; Chen, S.; Liu, Y.; Wang, L.; Huang, R. Impact of the March Arctic Oscillation on the South China Sea summer monsoon onset. *Int. J. Climatol.* **2021**, *41*, E3239–E3248. [CrossRef]

20. Luo, M.; Leung, Y.; Graf, H.F.; Herzog, M.; Zhang, W. Interannual variability of the onset of the South China Sea summer monsoon. *Int. J. Climatol.* **2016**, *36*, 550–562. [CrossRef]
21. Zhang, R.; Min, Q.; Su, J. Impact of El Niño on atmospheric circulations over East Asia and rainfall in China: Role of the anomalous western North Pacific anticyclone. *Sci. China Earth Sci.* **2017**, *60*, 1124–1132. [CrossRef]
22. Lu, R.Y.; Oh, J.H.; Kim, B.J. A teleconnection pattern in upper-level meridional wind over the North African and Eurasian continent in summer. *Tellus A* **2002**, *54*, 44–55. [CrossRef]
23. Kosaka, Y.; Nakamura, H.; Watanabe, M.; Kimoto, M. Analysis on the dynamics of a wave-like teleconnection pattern along the summertime Asian jet based on a reanalysis dataset and climate model simulations. *J. Meteor. Soc. Jpn.* **2009**, *87*, 561–580. [CrossRef]
24. Yasui, S.; Watanabe, M. Forcing Processes of the Summertime Circumglobal Teleconnection Pattern in a Dry AGCM. *J. Clim.* **2010**, *23*, 2093–2114. [CrossRef]
25. Hong, X.W.; Lu, R.Y. The meridional displacement of the summer Asian jet, Silk Road Pattern, and tropical SST anomalies. *J. Clim.* **2016**, *29*, 3753–3766. [CrossRef]
26. Xue, X.; Chen, W.; Hou, S. The long-term variation in the South Asia High intensity measured by 150-hPa eddy geopotential height. *Meteorol. Atmos. Phys.* **2020**, *132*, 833–844. [CrossRef]
27. Guan, W.N.; Hu, H.B.; Ren, X.J.; Yang, X.Q. Subseasonal zonal variability of the western Pacific subtropical high in summer: Climate impacts and underlying mechanisms. *Clim. Dyn.* **2019**, *53*, 3325–3344. [CrossRef]
28. Liu, B.; Zhu, C. Extremely late onset of the 2018 South China Sea summer monsoon following a La Niña event: Efects of triple SST anomaly mode in the North Atlantic and a weaker Mongolian cyclone. *Geophys. Res. Lett.* **2019**, *46*, 2956–2963. [CrossRef]
29. Huang, R.; Liu, Y.; Feng, T. Interdecadal change of summer precipitation over Eastern China around the late-1990s and associated circulation anomalies, internal dynamical causes. *Chin. Sci. Bull.* **2013**, *58*, 1339–1349. [CrossRef]
30. Wang, L.; Xu, P.Q.; Chen, W.; Liu, Y. Interdecadal Variations of the Silk Road Pattern. *J. Clim.* **2017**, *30*, 9915–9932. [CrossRef]
31. Mai, R.; Wen, M.; Zhang, R.H.; Li, L. The influence of wave trains in mid-high latitudes on persistent heavy rain during the first rainy season over South China. *Clim. Dyn.* **2019**, *53*, 2949–2968.
32. Hong, X.W.; Lu, R.Y.; Li, S.L. Asymmetric relationship between the meridional displacement of the Asian Westerly Jet and the Silk Road Pattern. *Adv. Atmos. Sci.* **2018**, *35*, 389–396. [CrossRef]
33. Hsu, H.H.; Lin, S.M. Asymmetry of the Tripole Rainfall Pattern during the East Asian Summer. *J. Clim.* **2007**, *20*, 4443–4458. [CrossRef]
34. Hu, P.; Chen, W.; Chen, S.; Liu, Y.; Wang, L.; Huang, R. Impact of the September Silk Road Pattern on the South China Sea summer monsoon withdrawal. *Int. J. Climatol.* **2020**, *40*, 6361–6368. [CrossRef]
35. Deng, K.; Yang, S.; Gu, D. Record-breaking heat wave in southern China and delayed onset of South China Sea summer monsoon driven by the Pacific subtropical high. *Clim. Dyn.* **2020**, *54*, 3751–3764. [CrossRef]
36. Kalnay, E.; Kanamitsu, M.; Kistler, R.; Collins, W.; Deaven, D.; Gandin, L.; Iredell, M.; Saha, S.; White, G.; Woollen, J. The NCEP/NCAR 40-year reanalysis project. *Bull. Amer. Meteor. Soc.* **1996**, *77*, 437–471. [CrossRef]
37. Xie, P.; Arkin, P.A. Global precipitation: A 17-year monthly analysis based on gauge observations, satellite estimates, and numerical model outputs. *Bull. Amer. Meteor. Soc.* **1997**, *78*, 2539–2558. [CrossRef]
38. Chen, S.; Yu, B.; Chen, W. An analysis on the physical process of the influence of AO on ENSO. *Clim. Dyn.* **2014**, *42*, 973–989. [CrossRef]
39. Chen, S.; Yu, B.; Chen, W. An interdecadal change in the influence of the spring Arctic oscillation on the subsequent ENSO around the early 1970s. *Clim. Dyn.* **2015**, *44*, 1109–1126. [CrossRef]
40. Hu, P.; Chen, W.; Huang, R.; Nath, D. On the weakening relationship between the South China Sea summer monsoon onset and crossequatorial flow after the late 1990s. *Int. J. Climatol.* **2018**, *38*, 3202–3208. [CrossRef]
41. Ding, S.Y.; Wen, Z.P.; Chen, W. Interdecadal change in the relationship between the South China Sea summer monsoon onset and two types of Pacific sea surface temperature anomaly. *Chin. J. Atmos. Sci.* **2016**, *40*, 243–256.
42. Hu, P.; Chen, W.; Chen, S.; Liu, Y.; Huang, R. Extremely Early Summer Monsoon Onset in the South China Sea in 2019 Following an El Niño Event. *Mon. Wea. Rev.* **2020**, *148*, 1877–1890. [CrossRef]
43. Xiang, B.; Wang, B. Mechanisms for the advanced Asian summer monsoon onset since the mid-to-late 1990s. *J. Clim.* **2013**, *26*, 1993–2009. [CrossRef]
44. Grinsted, A.; Moore, J.C.; Jevrejeva, S. Application of the Cross Wavelet Transform and Wavelet Coherence to Geophysical Time Series. *Nonlin. Process. Geophys.* **2004**, *11*, 561–566. [CrossRef]
45. Yuan, F.; Chen, W. Roles of the tropical convective activities over different regions in the earlier onset of the South China Sea summer monsoon after 1993. *Theor. Appl. Climatol.* **2013**, *113*, 175–185. [CrossRef]
46. North, G.R.; Bell, T.L.; Cahalan, R.F.; Moend, F.J. Sampling errors in the estimation of empirical orthogonal functions. *Mon. Wea. Rev.* **1982**, *110*, 699–706. [CrossRef]
47. Takaya, K.; Nakamura, H. A Formulation of a Phase-Independent Wave-Activity Flux for Stationary and Migratory Quasi-geostrophic Eddies on a Zonally Varying Basic Flow. *J. Atmos. Sci.* **2001**, *58*, 608–627. [CrossRef]
48. Liu, B.; Zhu, C. A possible precursor of the South China Sea summer monsoon onset: Effect of the South Asian High. *Geophys. Res. Lett.* **2016**, *43*, 11072–11079. [CrossRef]